

Chaos in Dirac Electron Optics: Emergence of a Relativistic Quantum ChimeraHong-Ya Xu,¹ Guang-Lei Wang,¹ Liang Huang,² and Ying-Cheng Lai^{1,*}¹*School of Electrical, Computer, and Energy Engineering, Arizona State University, Tempe, Arizona 85287-5706, USA*²*School of Physical Science and Technology, and Key Laboratory for Magnetism and Magnetic Materials of MOE, Lanzhou University, Lanzhou, Gansu 730000, China*

(Received 2 January 2018; published 23 March 2018)

We uncover a remarkable quantum scattering phenomenon in two-dimensional Dirac material systems where the manifestations of both classically integrable and chaotic dynamics emerge simultaneously and are electrically controllable. The distinct relativistic quantum fingerprints associated with different electron spin states are due to a physical mechanism analogous to a chiroptical effect in the presence of degeneracy breaking. The phenomenon mimics a chimera state in classical complex dynamical systems but here in a relativistic quantum setting—henceforth the term “Dirac quantum chimera,” associated with which are physical phenomena with potentially significant applications such as enhancement of spin polarization, unusual coexisting quasibound states for distinct spin configurations, and spin selective caustics. Experimental observations of these phenomena are possible through, e.g., optical realizations of ballistic Dirac fermion systems.

DOI: [10.1103/PhysRevLett.120.124101](https://doi.org/10.1103/PhysRevLett.120.124101)

The tremendous development of two-dimensional (2D) Dirac materials such as graphene, silicene, and germanene [1–5], in which the low-energy excitations follow the relativistic energy-momentum relation and obey the Dirac equation, has led to the emergence of a new area of research: Dirac electron optics [6–33]. Theoretically, it was articulated early [7] that Klein tunneling and the unique gapless conical dispersion relation can be exploited to turn a simply p - n junction into a highly transparent focusing lens with a gate-controlled *negative refractive index*, producing a Veselago lens for the chiral Dirac fermions in graphene. The negative refraction of Dirac fermions obeys the Snell’s law in optics and the angularly resolved transmittances in analogy with the Fresnel coefficients in optics have been recently confirmed experimentally [20,26]. Other works include various Klein-tunneling junction based electronic counterparts of optical phenomena such as Fabry-Pérot resonances [8,13], cloaking [11,14], waveguides [12,19], the Goos-Hänchen effect [9], the Talbot effect [22], beam splitter and collimation [21,28,29], and even the Dirac fermion microscope [33]. A Dirac material based electrostatic potential junction with a closed interface can be effectively tuned to optical guiding and acts as an unusual quantum electron-optics element whose effective refractive index can be electrically modulated, in which phenomena such as gate controlled caustics [6], electron Mie scattering [15,23–25], and whispering gallery modes [17,18,30,31] can arise. In addition, unconventional electron optical elements have been demonstrated such as valley resolved waveguides [34,35] and beam splitters [27], electronic birefringent superlens [16], and spin (current) lens [10,32]. Research on Dirac electron

optics offers the possibility to control Dirac electron flows in a similar way as for light.

In this Letter, we address the role of chaos in Dirac electron optics. In nonrelativistic quantum mechanics, the interplay between chaos and quantum optics has been studied in microcavity lasers [36–39] and deformed dielectric microcavities with non-Hermitian physics and wave chaos [40]. With the development of Dirac electron optics [6–33], the relativistic electronic counterparts of deformed optical dielectric cavities or resonators have become accessible. For massless Dirac fermions in ballistic graphene, the interplay between classical dynamics and electrostatic confinement has been studied [41–44] with the finding that integrable dynamics lead to sharp transport resonances due to the emergence of bound states while chaos typically removes the resonances. In these works, the uncharged degree of freedom such as electron spin, which is fundamental to relativistic quantum systems, was not treated.

Our focus is on the interplay between ray-path defined classical dynamics and spin in Dirac electron optical systems. To be concrete, we introduce an electrical gate potential defined junction with a ring geometry, in analogy to a dielectric annular cavity. Classically, this system generates integrable and mixed dynamics with the chaotic fraction of the phase space depending on the ring eccentricity and the effective refractive index configuration, where the index can be electrically tuned to negative values to enable Klein tunneling. Inside the gated region, the electron spin degeneracy is lifted through an exchange field from induced ferromagnetism, leading to a class of spin-resolved, electrically tunable quantum systems of

electron optics with massless Dirac fermions (by mimicking the photon polarization resolved photonic cavities made from synthesized chiral metamaterials). We develop an analytic wave function matching solution scheme and uncover a striking quantum scattering phenomenon: manifestations of classically integrable and chaotic dynamics coexist simultaneously in the system at the same parameter setting, which mimics a chimera state in classical complex dynamical systems [45–52]. The basic underlying physics is the well-defined, spin-resolved, gate-controllable refraction index that dominantly controls the ballistic motion of short-wavelength Dirac electrons across the junction interface, in which the ray tracing of reflection and refraction associated with particles belonging to different spin states generates distinct classical dynamics inside the junction or scatterer. Especially, with a proper gate potential, the spin-dependent refractive index profile can be controlled to generate regular ray dynamics for one spin state but generically irregular behavior with chaos for the other. A number of highly unusual physical phenomena arise, such as enhanced spin polarization with chaos, simultaneous quasicarried and whispering gallery type of resonances, and spin-selective lensing with a starkly near-field separation between the local density of states (DOS) for spin-up and spin-down particles.

Low energy excitations in 2D Dirac materials are described by the Dirac-Weyl Hamiltonian $H_0 = v_F \boldsymbol{\sigma} \cdot \mathbf{p}$, where v_F is the Fermi velocity, $\mathbf{p} = (p_x, p_y)$ is the momentum measured from a given Dirac point, and $\boldsymbol{\sigma} = (\sigma_x, \sigma_y)$ are Pauli matrices for sublattice pseudospin. In the presence of a gate potential and an exchange field due to the locally induced ferromagnetism inside the whole gated region, the effective Hamiltonian is $H = v_F s_0 \otimes \boldsymbol{\sigma} \cdot \mathbf{p} + s_0 \otimes \sigma_0 \mathcal{V}_{\text{gate}}(\mathbf{r}) - s_z \otimes \sigma_0 \mathcal{M}(\mathbf{r})$, where the Pauli matrix s_z acts on the real electron spin space, s_0 and σ_0 both are identity matrices, $\mathcal{V}_{\text{gate}}(\mathbf{r})$ and $\mathcal{M}(\mathbf{r})$ are the electrostatic and exchange potential, respectively. Because of the pseudospin-momentum locking (i.e., $\boldsymbol{\sigma} \cdot \mathbf{p}$), a nonuniform potential couples the two pseudospinor components, but the electron spin components are not coupled with each other. The exchange field breaks the twofold spin degeneracy. Since $[s_z \otimes \sigma_0, H] = 0$, the Hamiltonian can be simplified as $H_s = H_0 + \mathcal{V}_{\text{gate}}(\mathbf{r}) - s \mathcal{M}(\mathbf{r})$ with $s = \pm$ denoting the electron spin quantum number. Because of \mathcal{M} , the Dirac-type Hamiltonian H_s can give rise to spin dependent physical processes.

For the ring configuration in Fig. 1(a) and assuming the potentials are smooth on the scale of the lattice spacing but sharp in comparison with the conducting carriers' wavelength, in the polar coordinates $\mathbf{r} = (r, \theta)$, we have $\mathcal{V}_{\text{gate}}(\mathbf{r}) = \hbar v_F \nu_1 \Theta(R_1 - r) \Theta(|\mathbf{r} - \boldsymbol{\xi}| - R_2) + \hbar v_F \nu_2 \Theta(R_2 - |\mathbf{r} - \boldsymbol{\xi}|)$, and $\mathcal{M}(\mathbf{r}) = \hbar v_F \mu \Theta(R_1 - r)$, where Θ is the Heaviside step function, R_2 is the radius of the small disk gated region of strength $\hbar v_F (\nu_2 - \nu_1)$ placed inside a larger disk of radius R_1 ($> R_2$) and strength $\hbar v_F \nu_1$, the displacement vector between

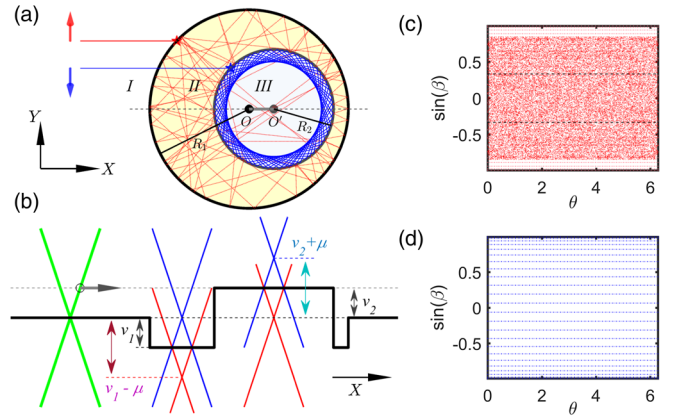


FIG. 1. Scattering system and classical ray dynamics. (a) Annular shaped scattering region with eccentricity $\xi = OO'$, (b) a cross-sectional view, (c), (d) chaotic and integrable ray dynamics on the Poincaré surface of section defined by the Birkhoff coordinates $(\theta, \sin\beta)$ for spin-up and -down particles, respectively, where θ denotes the polar angle of a ray's intersection point with the cavity boundary and β is the angle of incidence with respect to the boundary normal. The quantity $\sin\beta$ is proportional to the angular momentum and the critical lines for total internal reflection are given by $\sin\beta_c = \pm 1/n_s$.

the disk centers is $\boldsymbol{\xi} = (\xi, 0)$, and the exchange potential has the strength $\hbar v_F \mu$ over the whole gated region. The two circular boundaries divide the domain into three distinct regions: I: $r > R_1$; II: $r < R_1$ and $|\mathbf{r} - \boldsymbol{\xi}| > R_2$; III: $|\mathbf{r} - \boldsymbol{\xi}| < R_2$. For given particle energy $E = \hbar v_F \epsilon$, the momenta in the respective regions are $k_s^I = |\epsilon|$, $k_s^{II} = |\epsilon - \nu_1 + s\mu|$, and $k_s^{III} = |\epsilon - \nu_2 + s\mu|$. Within the gated region, the exchange potential splits the Dirac cone into two in the vertical direction in the energy domain while the electrostatic potential simply shifts the cone, leading to a spin-resolved, gate-controllable annular junction for massless Dirac electrons.

In the short wavelength limit, locally the curved junction interface appears straight for the electrons, so the gated regions and the surroundings can be treated as optical media. The unusual feature here is that the refractive indices are spin dependent: $n_s^{II,III} = (\epsilon + s\mu - \nu_{1,2})/\epsilon$, similar to light entering and through a polarization resolved photonic crystal [53,54]. Given the values of ϵ and μ , depending on the values of $\nu_{1,2}$, the refractive indices for the two spin states can be quite distinct with opposite signs. The system is thus analogous to a chiral photonic metamaterial based cavity, which represents a novel class of Dirac electron optics systems.

The classical behaviors of Dirac-like particles in the short wavelength limit can be assessed using the optical analogy, as done previously for circularly curved p - n junctions [6,33], where the classical trajectories are defined via the principle of least time. Because of the spin dependent and piecewise constant nature of the index profile, the resulting stationary ray paths for the Dirac

electrons are spin-resolved and consist of straight line segments. At a junction interface, there is ray splitting governed by the spin-resolved Snell's law. On a Poincaré surface of the section, the classical dynamics are described by a spin-resolved map F_s relating the dynamical variables θ and β (Fig. 1) between two successive collisions with the interface: $(\theta_i, \sin \beta_i) \mapsto (\theta_{i+1}, \sin \beta_{i+1})$. The ray-splitting picture is adequate for uncovering the relativistic quantum fingerprints of distinct classical dynamics.

Spin-resolved ray trajectories inside the junction lead to the simultaneous coexistence of distinct classical dynamics. For example, for the parameter setting $\nu_2 = -\nu_1 = \epsilon = \mu$, i.e., $n_s^{\text{II}} = 2 + s$ and $n_s^{\text{III}} = s$, for spin-up particles ($s = +$), the junction is an eccentric annular electron cavity characterized by the refractive indices $n_+^{\text{II}} = 3$ and $n_+^{\text{III}} = 1$, as exemplified in Fig. 1(b) for $\xi = 0.3$. However, for spin-down particles ($s = -$), the junction appears as an off-centered negatively refracted circular cavity with $n_-^{\text{II}} = 1$ and $n_-^{\text{III}} = -1$. Figures 1(c) and 1(d) show the corresponding ray dynamics on the Poincaré surface of section for spin-up and -down particles, respectively, where the former exhibit chaos while the dynamics associated with the latter are integrable with angular momentum being the second constant of motion.

For a spin unpolarized incident beam, the simultaneous occurrence of integrable and chaotic classical dynamics means the coexistence of distinct quantum manifestations, leading to the emergence of a Dirac quantum chimera. To establish this, we carry out a detailed analysis of the scattering matrices for spin-dependent, relativistic quantum scattering and transport through the junction. Using insights from analyzing optical dielectric cavities [55,56] and nonrelativistic quantum billiard systems [57,58], we develop an analytic wave function matching scheme at the junction interfaces (See Supplemental Material [59] which includes Refs. [24,30,60–64]) to solve the Dirac-Weyl equation to obtain the scattering matrix S as a function of the energy E as well as the spin polarization s for given system parameters R_2/R_1 , ξ , $\nu_{1,2}$, and μ . The Wigner-Smith time delay [60,61] is defined from the S matrix as $\tau = -i\hbar \text{Tr}[S^\dagger (\partial S / \partial E)]$, which is proportional to the DOS of the cavity. Large positive values of τ signify resonances associated with the quasibound states [65]. Physically, a sharper resonance corresponds to a longer trapping lifetime and scattering time delay. Previous works on wave or quantum chaotic scattering [66–85] established that classical chaos can smooth out (broaden) the sharp resonances and reduce the time delay markedly while integrable dynamics can lead to stable, long-lived bound states (or trapping modes).

We present concrete evidence for Dirac quantum chimera. Figure 2(a) shows, for $R_2/R_1 = 0.6$, $\mu = -\nu_1 = 5$, and $\nu_2 = 45$, the dimensionless time delay (on a logarithmic scale) versus the eccentricity ξ and energy E (in units of $\hbar v_F/R_1$). Figure 2(b) shows the maximum time delay

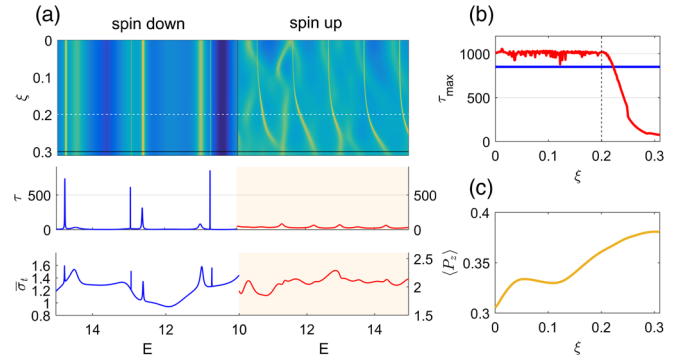


FIG. 2. A Dirac quantum chimera. (a) Top: Contour map of dimensionless Wigner-Smith time delay (on a logarithmic scale) versus energy E and eccentricity ξ for spin-down (left) and -up (right) cases, where the bright yellow color indicates larger values. Middle and bottom panels: time delay and total cross section averaged over all directions of the incident waves versus E , respectively, for $\xi = 0.3$. (b) Dependence of the maximum time delay on ξ (red: spin-up; blue: spin-down). (c) Energy averaged spin polarization versus ξ .

[within the given energy range in Fig. 2(a)] versus ξ for spin-up (red) and spin-down (blue) particles. There are drastic changes in the time delay as the energy is varied, which are characteristic of well-isolated, narrow resonances and imply the existence of relatively long-lived confined modes. There is a key difference in the resonances associated with the spin-up and -down states: the former depend on the eccentricity parameter ξ and are greatly suppressed for $\xi > 0.2$, while the latter are independent of ξ . For example, the middle panel of Fig. 2(a) shows that, for a severely deformed structure ($\xi = 0.3$), there are sharp resonances with high peak values of the time delay for the spin down state, but none for the spin-up state. The suppression of resonances associated with the spin-up state is consistent with the behavior of the total cross section $\bar{\sigma}_t$ (averaged over the directions of the incident wave) given in terms of the S -matrix elements by $\bar{\sigma}_t = (2k)^{-1} \sum_{m,l=-\infty}^{\infty} |S_{ml} - \delta_{ml}|^2$, as shown in the bottom panel of Fig. 2(a). Because the classical dynamics for massless fermions in the spin-up and -down states are chaotic and integrable, respectively [cf., Figs. 1(c), 1(d)], there is *simultaneous* occurrence of two characteristically different quantum scattering behaviors for a spin unpolarized beam: one without and another with *sharp* resonances. This striking contrast signifies a Dirac quantum chimera.

Are there unexpected, counterintuitive physical phenomena associated with a Dirac quantum chimera? Yes, there are. Here we present two and point out their applied values.

The first is spin polarization enhancement, which has potential applications to Dirac material based spintronics. A general way to define spin polarization is through the spin conductivities $G^{\downarrow(\uparrow)}$ as $P_z = (G^\downarrow - G^\uparrow)/(G^\downarrow + G^\uparrow)$. Imagine a system consisting of a set of sparse, randomly distributed, identical junction-type of annular scatterers,

and assume that the scatterer concentration is sufficiently low ($n_c \ll 1/R_1^2$) so that multiple scattering events can be neglected. In this case, the spin conductivities can be related to the transport cross section as $G^{\downarrow(\uparrow)}/G_0 = k/(n_c \sigma_{\text{tr}}^{\downarrow(\uparrow)})$, where G_0 is the conductance quantum and $\sigma_{\text{tr}}^{\downarrow(\uparrow)}$ can be calculated from the S matrix. For a spin unpolarized incident beam along the x axis with equal spin-up and -down populations, we calculate the average spin polarization over a reasonable Fermi energy range as a function of the eccentricity ξ , as shown in Fig. 2(c). For $\xi > 0.2$ so classical chaos is relatively well developed and a Dirac quantum chimera emerges, there is robust enhancement of spin polarization. From the standpoint of classical dynamics, the scattering angle is much more widely distributed for spin-up particles (due to chaos) as compared with the angle distribution for spin-down particles with integrable dynamics, leading to a larger effective resistance for spin-up particles. From an applied perspective, the enhancement of spin polarization brought about by a Dirac quantum chimera can be exploited for developing spin rheostats or filters, where one of the spin resistances, e.g., $R^\uparrow \propto 1/G^\uparrow$, can be effectively modulated through tuning the deformation parameter ξ so as to induce classically

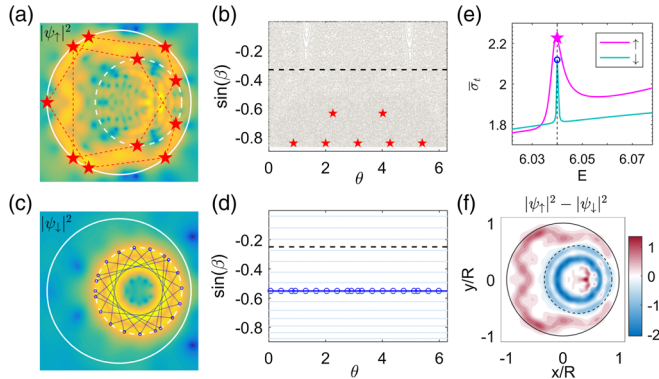


FIG. 3. Spin polarized scarred and regular whispering-gallery-mode resonances as a result of Dirac quantum chimera. (a), (c) Real space probability densities (on a logarithmic scale) of the representative quasibound states for spin-up and spin-down Dirac electrons, respectively. For the spin-up particles, the spinor wave solution is scarred by an unstable periodic ray trajectory obeying the Snell's law, as indicated by the red-dashed path with highlighted pentagram markers. The spin-down Dirac electrons are associated with a whispering gallery ray path due to the continuous total internal reflections denoted by the blue dotted segments. (b), (d) The corresponding phase-space representations with regions below the critical black dashed lines satisfying the total internal reflection at the boundary. The distinct quasibound modes are from simultaneous resonances under the same system parameters, leading to a relativistic quantum chimera. Further signatures of the chimera state can be seen in the plot of the total cross section versus the particle energy for different spin states (e) and a net spin distribution with a dramatic spin-resolved separation in the real space confined inside the cavity (f).

chaotic motion for one type of polarization but integrable dynamics for another.

The second phenomenon is resonance and lensing associated with a Dirac quantum chimera. Figures 3(a)–3(f) show, for $\xi = 0.27$ (in units of R_1), $R_2/R_1 = 0.6$, $\nu_2 = 4\nu_1 = -4\mu = 24.16$ (in units of $1/R_1$) and $E = 6.04$ (in units of $\hbar v_F/R_1$), a resonant (quasibound) state, in which the spatially separated, spin-resolved local DOS is confined inside the cavity. The spin-up state is concentrated about a particular unstable periodic orbit without the rotational symmetry [Figs. 3(a) and 3(b)] and exhibits a scarring pattern with a relatively short lifetime characterized by a wider resonance profile, as shown in Fig. 3(e). Spin-down particles are trapped inside the inner disk by a regular long-lived whispering gallery mode associated with the integrable dynamics [Figs. 3(c) and 3(d)]. The Dirac quantum chimera thus manifests itself as the simultaneous occurrence of a magnetic scarred quasibound state and a whispering gallery mode excited by an incident wave with equal populations of spin-up and -down particles, as shown in Fig. 3(f), a color-coded spatial distribution of the difference between the local DOS for spin-up and -down particles.

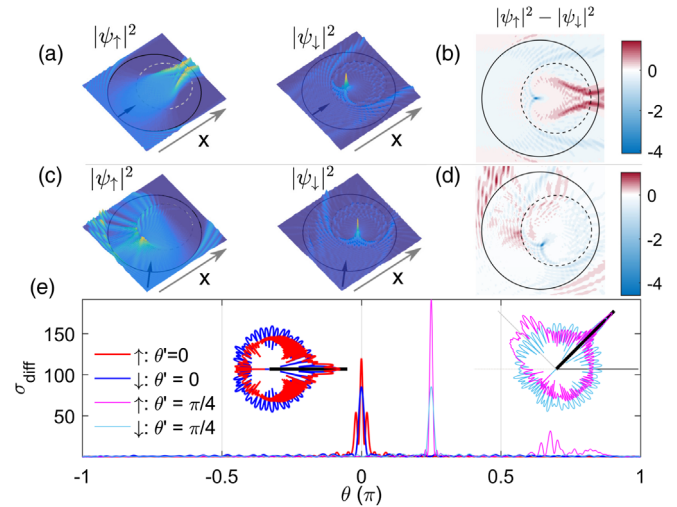


FIG. 4. Spin-selective caustic lens and skew scattering associated with a Dirac quantum chimera. (a) Caustic patterns resulting from the scattering of a spin unpolarized planar incident wave traveling along the positive x axis ($\theta' = 0$) with relatively short wavelength, i.e., $kR_1 = 70 \gg 1$, and (c) from scattering of the wave propagating along the direction that makes an angle $\theta' = \pi/4$ with the x axis. (b), (d) The corresponding spatially resolved near field net spin distributions measured by the difference $|\psi_\uparrow|^2 - |\psi_\downarrow|^2$, respectively. (e) The resulting far-field behavior characterized by the angular distributions of spin-dependent differential cross sections with symmetric profiles for $\theta' = 0$ (left inset) and a spin-selective asymmetric one for $\theta' = \pi/4$ (right inset), where both insets are plotted by the eighth root of $\sigma_{\text{diff}}^{\uparrow(\downarrow)}$ in order to weaken the drastic contrast variation in magnitude for better visualization. Parameters are $\xi = 0.27$, $R_2/R_1 = 0.6$, $\nu_2 = \mu = -\nu_1 = 70$, and $E = 70$.

In the sufficiently short wavelength regime where the ray picture becomes accurate, a spin-resolved lensing behavior arises, due to the simultaneous occurrence of two distinct quantum states associated with the chimera state. The cavity can be regarded as an effective electronic Veselago lens with a robust caustic function for spin-down particles but the spin-up particles encounter simply a conventional lens of an irregular shape. Particularly, for a spin-unpolarized, planar incident wave, a spin-selective caustic behavior arises, as shown in Figs. 4(a)–4(d) through the color-coded near-field patterns. There is a pronounced lensing caustic of the cusp type for the spin-down state while a qualitatively distinct lensing pattern occurs for the spin-up state. A consistent far-field angular distribution of the differential cross section is shown in Fig. 4(e), which gives rise to well-oriented or -collimated, spin-dependent far-field scattering with the angle resolved profile minimized into a small range due to the lensing effect. Despite a lack of robust lensing, the spin-up particles in general undergo asymmetric scattering, which can lead to spin-polarized transverse transport in addition to longitudinal spin filtering.

To summarize, we uncover a Dirac quantum chimera—a type of relativistic quantum scattering states characterized by the simultaneous coexistence of two distinct types of behaviors as the manifestations of classical chaotic and integrable dynamics, respectively. The physical origin of the chimera state is the optical-like behavior of massless Dirac fermions with both spin and pseudospin degrees of freedom, which together define a spin-resolved Snell's law governing the chiral particles' ballistic motion. The phenomenon is predicted analytically based on quantum scattering from a gate-defined annular junction structure. The chimera has striking physical consequences such as spin polarization enhancement, unusual quantum resonances, and spin-selective lensing, which are potentially exploitable for developing 2D Dirac material-based electronic and spintronic devices.

We would like to acknowledge support from the Vannevar Bush Faculty Fellowship program sponsored by the Basic Research Office of the Assistant Secretary of Defense for Research and Engineering and funded by the Office of Naval Research through Grant No. N00014-16-1-2828. L. H. is also supported by NNSF of China under Grant No. 11775101.

*Ying-Cheng.Lai@asu.edu

- [1] K. S. Novoselov, A. K. Geim, S. V. Morozov, D. Jiang, Y. Zhang, S. V. Dubonos, I. V. Grigorieva, and A. A. Firsov, *Science* **306**, 666 (2004).
- [2] K. S. Novoselov, A. K. Geim, S. V. Morozov, D. Jiang, M. I. Katsnelson, I. V. Grigorieva, S. V. Dubonos, and A. A. Firsov, *Nature (London)* **438**, 197 (2005).
- [3] A. H. C. Neto, F. Guinea, N. M. R. Peres, K. S. Novoselov, and A. K. Geim, *Rev. Mod. Phys.* **81**, 109 (2009).
- [4] T. Wehling, A. Black-Schaffer, and A. Balatsky, *Adv. Phys.* **63**, 1 (2014).
- [5] J. Wang, S. Deng, Z. Liu, and Z. Liu, *Nat. Sci. Rev.* **2**, 22 (2015).
- [6] J. Cserti, A. Pályi, and C. Péterfalvi, *Phys. Rev. Lett.* **99**, 246801 (2007).
- [7] V. V. Cheianov, V. Fal'ko, and B. L. Altshuler, *Science* **315**, 1252 (2007).
- [8] A. V. Shytov, M. S. Rudner, and L. S. Levitov, *Phys. Rev. Lett.* **101**, 156804 (2008).
- [9] C. W. J. Beenakker, R. A. Sepkhanov, A. R. Akhmerov, and J. Tworzydło, *Phys. Rev. Lett.* **102**, 146804 (2009).
- [10] A. G. Moghaddam and M. Zareyan, *Phys. Rev. Lett.* **105**, 146803 (2010).
- [11] N. Gu, M. Rudner, and L. Levitov, *Phys. Rev. Lett.* **107**, 156603 (2011).
- [12] J. R. Williams, T. Low, M. S. Lundstrom, and C. M. Marcus, *Nat. Nanotechnol.* **6**, 222 (2011).
- [13] P. Rickhaus, R. Maurand, M.-H. Liu, M. Weiss, K. Richter, and C. Schönenberger, *Nat. Commun.* **4**, 2342 (2013).
- [14] B. Liao, M. Zebarjadi, K. Esfarjani, and G. Chen, *Phys. Rev. B* **88**, 155432 (2013).
- [15] R. L. Heinisch, F. X. Bronold, and H. Fehske, *Phys. Rev. B* **87**, 155409 (2013).
- [16] M. M. Asmar and S. E. Ulloa, *Phys. Rev. B* **87**, 075420 (2013).
- [17] J.-S. Wu and M. M. Fogler, *Phys. Rev. B* **90**, 235402 (2014).
- [18] Y. Zhao, J. Wyrick, F. D. Natterer, J. F. Rodriguez-Nieva, C. Lewandowski, K. Watanabe, T. Taniguchi, L. S. Levitov, N. B. Zhitenev, and J. A. Stroscio, *Science* **348**, 672 (2015).
- [19] P. Rickhaus, M.-H. Liu, P. Makk, R. Maurand, S. Hess, S. Zihlmann, M. Weiss, K. Richter, and C. Schonenberger, *Nano Lett.* **15**, 5819 (2015).
- [20] G.-H. Lee, G.-H. Park, and H.-J. Lee, *Nat. Phys.* **11**, 925 (2015), letter.
- [21] P. Rickhaus, P. Makk, K. Richter, and C. Schonenberger, *Appl. Phys. Lett.* **107**, 251901 (2015).
- [22] J. D. Walls and D. Hadad, *Sci. Rep.* **6**, 26698 (2016).
- [23] J. Caridad, S. Connaughton, C. Ott, H. B. Weber, and V. Krstic, *Nat. Commun.* **7**, 12894 (2016).
- [24] C. Gutierrez, L. Brown, C.-J. Kim, J. Park, and A. N. Pasupathy, *Nat. Phys.* **12**, 1069 (2016).
- [25] J. Lee, D. Wong, J. Velasco Jr., J. F. Rodriguez-Nieva, S. Kahn, H.-Z. Tsai, T. Taniguchi, K. Watanabe, A. Zettl, F. Wang, L. S. Levitov, and M. F. Crommie, *Nat. Phys.* **12**, 1032 (2016).
- [26] S. Chen, Z. Han, M. M. Elahi, K. M. M. Habib, L. Wang, B. Wen, Y. Gao, T. Taniguchi, K. Watanabe, J. Hone, A. W. Ghosh, and C. R. Dean, *Science* **353**, 1522 (2016).
- [27] M. Settnes, S. R. Power, M. Brandbyge, and A.-P. Jauho, *Phys. Rev. Lett.* **117**, 276801 (2016).
- [28] M.-H. Liu, C. Gorini, and K. Richter, *Phys. Rev. Lett.* **118**, 066801 (2017).
- [29] A. W. Barnard, A. Hughes, A. L. Sharpe, K. Watanabe, T. Taniguchi, and D. Goldhaber-Gordon, *Nat. Commun.* **8**, 15418 (2017).

- [30] Y. Jiang, J. Mao, D. Moldovan, M. R. Masir, G. Li, K. Watanabe, T. Taniguchi, F. M. Peeters, and E. Y. Andrei, *Nat. Nanotechnol.* **12**, 1045 (2017).
- [31] F. Ghahari, D. Walkup, C. Gutiérrez, J. F. Rodriguez-Nieva, Y. Zhao, J. Wyrick, F. D. Natterer, W. G. Cullen, K. Watanabe, T. Taniguchi, L. S. Levitov, N. B. Zhitenev, and J. A. Stroschio, *Science* **356**, 845 (2017).
- [32] S.-H. Zhang, J.-J. Zhu, W. Yang, and K. Chang, *2D Mater.* **4**, 035005 (2017).
- [33] P. Bäggi, J. M. Caridad, C. Stampfer, G. Calogero, N. R. Papior, and M. Brandbyge, *Nat. Commun.* **8**, 15783 (2017).
- [34] Z. Wu, F. Zhai, F. M. Peeters, H. Q. Xu, and K. Chang, *Phys. Rev. Lett.* **106**, 176802 (2011).
- [35] F. Zhai, Y.-L. Ma, and K. Chang, *New J. Phys.* **13**, 083029 (2011).
- [36] J. U. Nöckel, A. D. Stone, G. Chen, H. L. Grossman, and R. K. Chang, *Opt. Lett.* **21**, 1609 (1996).
- [37] J. U. Nöckel and A. D. Stone, *Nature (London)* **385**, 45 (1997).
- [38] C. Gmachl, F. Capasso, E. E. Narimanov, J. U. Nöckel, A. D. Stone, J. Faist, D. L. Sivco, and A. Y. Cho, *Science* **280**, 1556 (1998).
- [39] K. J. Vahala, *Nature (London)* **424**, 839 (2003).
- [40] H. Cao and J. Wiersig, *Rev. Mod. Phys.* **87**, 61 (2015).
- [41] J. H. Bardarson, M. Titov, and P. W. Brouwer, *Phys. Rev. Lett.* **102**, 226803 (2009).
- [42] M. Schneider and P. W. Brouwer, *Phys. Rev. B* **84**, 115440 (2011).
- [43] J. Heintl, M. Schneider, and P. W. Brouwer, *Phys. Rev. B* **87**, 245426 (2013).
- [44] M. Schneider and P. W. Brouwer, *Phys. Rev. B* **89**, 205437 (2014).
- [45] Y. Kuramoto and D. Battogtokh, *Nonlinear Phenom. Complex Syst.* **5**, 380 (2002).
- [46] D. M. Abrams and S. H. Strogatz, *Phys. Rev. Lett.* **93**, 174102 (2004).
- [47] D. M. Abrams and S. H. Strogatz, *Int. J. Bifurcation Chaos Appl. Sci. Eng.* **16**, 21 (2006).
- [48] M. R. Tinsley, S. Nkomo, and K. Showalter, *Nat. Phys.* **8**, 662 (2012).
- [49] A. M. Hagerstrom, T. E. Murphy, R. Roy, P. Hövel, I. Omelchenko, and E. Schöll, *Nat. Phys.* **8**, 658 (2012).
- [50] E. A. Martens, S. Thutupalli, A. Fourrière, and O. Hallatschek, *Proc. Natl. Acad. Sci. U.S.A.* **110**, 10563 (2013).
- [51] N. Yao, Z.-G. Huang, Y.-C. Lai, and Z.-G. Zheng, *Sci. Rep.* **3**, 3522 (2013).
- [52] N. Yao, Z.-G. Huang, C. Grebogi, and Y.-C. Lai, *Sci. Rep.* **5**, 12988 (2015).
- [53] J. K. Gansel, M. Thiel, M. S. Rill, M. Decker, K. Bade, V. Saile, G. von Freymann, S. Linden, and M. Wegener, *Science* **325**, 1513 (2009).
- [54] S. Zhang, Y.-S. Park, J. Li, X. Lu, W. Zhang, and X. Zhang, *Phys. Rev. Lett.* **102**, 023901 (2009).
- [55] G. Hackenbroich and J. U. Nöckel, *Europhys. Lett.* **39**, 371 (1997).
- [56] M. Hentschel and K. Richter, *Phys. Rev. E* **66**, 056207 (2002).
- [57] E. Doron and U. Smilansky, *Nonlinearity* **5**, 1055 (1992).
- [58] E. Doron and S. D. Frisch, *Phys. Rev. Lett.* **75**, 3661 (1995).
- [59] See Supplemental Material at <http://link.aps.org/supplemental/10.1103/PhysRevLett.120.124101> for a detailed analytical derivation of the scattering matrix for the Dirac electron optical system with classically integrable or chaotic dynamics. Formulas for various characterizing quantities (e.g., scattering cross sections) and numerical validation are also included.
- [60] E. P. Wigner, *Phys. Rev.* **98**, 145 (1955).
- [61] F. T. Smith, *Phys. Rev.* **118**, 349 (1960).
- [62] H. Schomerus, M. Marciiani, and C. W. J. Beenakker, *Phys. Rev. Lett.* **114**, 166803 (2015).
- [63] D. Zwillinger, *Table of Integrals, Series, and Products* (Elsevier Science, New York, 2014).
- [64] P. Wei, S.-W. Lee, F. Lemaitre, L. Pinel, D. Cutaia, W.-J. Cha, F. Katmis, Y. Zhu, D. Heiman, J. Hone, and J. S. M. C. -T. Chen, *Nat. Mater.* **15**, 711 (2016).
- [65] S. Rotter and S. Gigan, *Rev. Mod. Phys.* **89**, 015005 (2017).
- [66] R. Blümel and U. Smilansky, *Phys. Rev. Lett.* **60**, 477 (1988).
- [67] R. Blümel and U. Smilansky, *Physica (Amsterdam)* **36D**, 111 (1989).
- [68] R. A. Jalabert, H. U. Baranger, and A. D. Stone, *Phys. Rev. Lett.* **65**, 2442 (1990).
- [69] C. M. Marcus, A. J. Rimberg, R. M. Westervelt, P. F. Hopkins, and A. C. Gossard, *Phys. Rev. Lett.* **69**, 506 (1992).
- [70] Y.-C. Lai, R. Blümel, E. Ott, and C. Grebogi, *Phys. Rev. Lett.* **68**, 3491 (1992).
- [71] R. Ketzmerick, *Phys. Rev. B* **54**, 10841 (1996).
- [72] T. Kottos and U. Smilansky, *Phys. Rev. Lett.* **79**, 4794 (1997).
- [73] A. S. Sachrajda, R. Ketzmerick, C. Gould, Y. Feng, P. J. Kelly, A. Delage, and Z. Wasilewski, *Phys. Rev. Lett.* **80**, 1948 (1998).
- [74] T. Kottos, U. Smilansky, J. Fortuny, and G. Nesti, *Radio Sci.* **34**, 747 (1999).
- [75] T. Kottos and U. Smilansky, *Phys. Rev. Lett.* **85**, 968 (2000).
- [76] B. Huckestein, R. Ketzmerick, and C. H. Lewenkopf, *Phys. Rev. Lett.* **84**, 5504 (2000).
- [77] G. Casati, I. Guarneri, and G. Maspero, *Phys. Rev. Lett.* **84**, 63 (2000).
- [78] A. P. S. de Moura, Y.-C. Lai, R. Akis, J. P. Bird, and D. K. Ferry, *Phys. Rev. Lett.* **88**, 236804 (2002).
- [79] R. Crook, C. G. Smith, A. C. Graham, I. Farrer, H. E. Beere, and D. A. Ritchie, *Phys. Rev. Lett.* **91**, 246803 (2003).
- [80] T. Kottos and U. Smilansky, *J. Phys. A* **36**, 3501 (2003).
- [81] S. Gnuzmann and U. Smilansky, *Adv. Phys.* **55**, 527 (2006).
- [82] R. Band, A. Sawicki, and U. Smilansky, *J. Phys. A* **43**, 415201 (2010).
- [83] Y. Krivolapov, S. Fishman, E. Ott, and T. M. Antonsen, *Phys. Rev. E* **83**, 016204 (2011).
- [84] R. Yang, L. Huang, Y.-C. Lai, and C. Grebogi, *Europhys. Lett.* **94**, 40004 (2011).
- [85] G. L. Wang, L. Ying, Y.-C. Lai, and C. Grebogi, *Phys. Rev. E* **87**, 052908 (2013).